EXAFS and HRTEM Evidence for As(III)-Containing Surface Precipitates on Nanocrystalline Magnetite: Implications for As Sequestration

Guillaume Morin,*,[†] Yuheng Wang,[†] Georges Ona-Nguema,[†] Farid Juillot,[†] Guillaume Calas,[†] Nicolas Menguy,[†] Emmanuel Aubry,[‡] John R. Bargar,[§] and Gordon E. Brown, Jr.[§,#]

[†]*Institut de Minéralogie et de Physique des Milieux Condensés (IMPMC), UMR 7590, CNRS, Université Paris 6, Université Paris 7, IPGP, 140 rue de Lourmel, 75015 Paris, France,* [‡]*Biogéochimie et Ecologie des Milieux Continentaux (Bioemco), UMR 7618, Université Paris 6, INRA, INAPG, CNRS, ENS, ENSCP Case 120, Tour 56, couloir 56-66, 4ème étage, 4 place Jussieu, 75252 Paris cedex 05, France,* [§]*Stanford Synchrotron Radiation Lightsource, SLAC National Accelerator Laboratory, 2575 Sand Hill Road, MS 69, Menlo Park, California 94025, and* [#]*Surface and Aqueous Geochemistry Group, Department of Geological and Environmental Sciences, Stanford University, Stanford, California 94305-2115*

Arsenic sorption onto iron oxide spinels such as magnetite could contribute to immobilization of arsenite (AsO_3^{3-}), the reduced, highly toxic form of arsenic in contaminated anoxic groundwaters, as well as to putative remediation processes. Nanocrystalline magnetite (< 20 nm) is known to exhibit higher efficiency for arsenite sorption than larger particles, sorbing as much as $\sim 20 \mu mol/m^2$ of arsenite. To improve our understanding of this process, we investigated the molecular level structure of As(III)-containing sorption products on two types of fine-grained magnetite: (1) a biogenic one with an average particle diameter of 34 nm produced by reduction of lepidocrocite (γ-FeOOH) by *Shewanella putrefaciens* and (2) a synthetic, abiotic, nanocrystalline magnetite with an average particle diameter of 11 nm. Results from extended X-ray absorption spectroscopy (EXAFS) for both types of magnetite with As(III) surface coverages of up to 5 $\mu mol/m^2$ indicate that As(III) forms dominantly inner-sphere, tridentate, hexanuclear, corner-sharing surface complexes (^3C) in which AsO_3 pyramids occupy vacant tetrahedral sites on octahedrally terminated {111} surfaces of magnetite. Formation of this type of surface complex results in a decrease in dissolved As(III) concentration below the maximum concentration level recommended by the World Health Organization (10 $\mu g/L$), which corresponds to As(III) surface coverages of 0.16 and 0.19 $\mu mol/m^2$ in our experiments. In addition, high-resolution transmission electron microscopy (HRTEM) coupled with energy dispersive X-ray spectroscopy (EDXS) analyses revealed the occurrence of an amorphous As(III)-rich surface precipitate forming at As(III) surface coverages as low as 1.61 $\mu mol/m^2$. This phase hosts the majority of adsorbed arsenite at surface coverages exceeding the theoretical maximum site density of vacant tetrahedral sites on the magnetite {111} surface (3.2 sites/nm^2 or 5.3 $\mu mol/m^2$). This finding helps to explain the exceptional As(III) sorption capacity of nanocrystalline magnetite particles ($> 10 \mu mol/m^2$). However, the higher solubility of the amorphous surface precipitate compared to the ^3C surface complexes causes a dramatic increase of dissolved As concentration for coverages above 1.9 $\mu mol/m^2$.

Introduction

Arsenic levels are above the maximum concentration level (MCL) recommended by the World Health Organization (WHO) (10 $\mu g/L$) in a number of groundwater resources, especially in Southeast Asian countries [1]. It is now accepted that bacterial reduction of As-bearing sediments in reducing aquifers is an important process affecting groundwater quality.[2,3] More specifically, highly toxic As(III) is thought to be released via reductive dissolution of As(V)-bearing ferric (oxyhydr)oxides,[2−5] which are common substrates for arsenic sorption in oxidizing media.[6] These adsorption properties have recently been exploited

to develop a simple, cost-effective means of removing arsenic from groundwater in rural environments in Bangladesh.[7] Arsenic-(III) has generally higher apparent solubility compared to As(V) in oxic and suboxic media,[2,8−11] although available experimental sorption and coprecipitation data show that As(III) strongly sorbs onto Fe-containing minerals, including Fe(II,III) biogenic minerals such as magnetite (Fe_3O_4),[12,13] hydroxycarbonate green-rust ($Fe^{II}_4Fe^{III}_2(OH)_{12}CO_3$), ferrous carbonate hydroxide ($Fe_2(OH)_2CO_3$), $Fe(OH)_2$,[14] pyrite (FeS_2), and troilite (FeS),[15]

*Corresponding author (telephone: 33-1-44-27-75-04; e-mail: guillaume. morin@impmc.jussieu.fr).

(1) Vaughan, D. J. *Elements* **2006**, *2*, 71−75.
(2) Charlet, L.; Polya, D. A. *Elements* **2006**, *2*, 91−96.
(3) Islam, F. S.; Gault, A. G.; Boothman, C.; Polya, D. A.; Charnock, J. M.; Chatterjee, D.; Lloyd, J. R. *Nature* **2004**, *430*, 68−71.
(4) Nickson, R.; McArthur, J.; Burgess, W.; Ahmed, K. M.; Ravenscroft, P.; Rahman, M. *Nature* **1998**, *395*, 338.
(5) Oremland, R. S.; Stolz, J. F. *Science* **2003**, *300*, 939−944.
(6) Morin, G.; Calas, G. *Elements* **2006**, *2*, 97−101.
(7) Sarkar, S.; Blaney, L. M.; Gupta, A.; Ghosh, D.; Sengupta, A. K. *Environ. Sci. Technol.* **2008**, *42*, 4268−4273.

(8) Ahmann, D.; Krumholz, L. R.; Hemond, H. F.; Lovley, D. R.; Morel, F. M. M. *Environ. Sci. Technol.* **1997**, *31*, 2923−2930.
(9) Jones, C. A.; Langner, H. W.; Anderson, K.; McDermott, T. R.; Inskeep, W. P. *Soil Sci. Soc. Am. J.* **2000**, *64*, 600−608.
(10) van Geen, A.; Rose, J.; Thoral, S.; Garnier, J. M.; Zheng, Y.; Bottero, J. Y. *Geochim. Cosmochim. Acta* **2004**, *68*, 3475−3486.
(11) Burnol, A.; Garrido, F.; Baranger, P.; Joulian, C.; Dictor, M.-C.; Bodenan, F.; Morin, G.; Charlet, L. *Geochem. Trans.* **2007**, *8*, 12−30.
(12) Dixit, S.; Hering, J. G. *Environ. Sci. Technol.* **2003**, *37*, 4182−4189.
(13) Wang, Y.; Morin, G.; Ona-Nguema, G.; Menguy, N.; Juillot, F.; Aubry, E.; Guyot, F.; Calas, G.; Brown, G. E., Jr. *Geochim. Cosmochim. Acta* **2008**, *72*, 2573−2586.
(14) Ona-Nguema, G.; Morin, G.; Wang, Y.; Menguy, N.; Juillot, F.; Olivi, L.; Aquilanti, G.; Abdelmoula, M.; Ruby, C.; Bargar, J. R.; Guyot, F.; Calas, G.; Brown, G. E., Jr. *Geochim. Cosmochim. Acta* **2009**, *73*, 1359−1381.
(15) Bostick, B. C.; Fendorf, S. *Geochim. Cosmochim. Acta* **2003**, *67*, 909−921.

which are common products of microbial reduction of ferric (oxyhydr)oxides.[16-19] Indeed, several studies have reported that the bioreduction of ferrihydrite ($Fe_5HO_8 \cdot 4H_2O$) into magnetite increased As(III) retention in batch experiments[20,21] as well as over short reaction times (20 days) in column experiments;[22,23] longer reaction times were found to result in progressive release of As due to leaching of Fe from ferrihydrite in the columns.[23]

Arsenic sorption on magnetite has recently been proposed as a possible water decontamination process[24] on the basis of the ability of As-sorbed magnetite particles to be harvested from a suspension using low-intensity magnetic fields. In addition, exceptional As(III) sorption capacities (up to 20 $\mu mol/m^2$) have been reported for nanocrystalline magnetite (12 nm).[24-26] Sorption capacities of 13 $\mu mol/m^2$ have also been reported recently for nanocrystalline (6 nm) maghemite (γ-Fe_2O_3)[27] and were interpreted as being due to purported differences in the surface structure of the nanocrystals versus those of larger maghemite particles. Because no equivalent data are available for magnetite, knowledge of the molecular level nature of As(III) complexes on the surface of nanoparticulate magnetite would help to explain their high As(III) sorption capacity. In addition, such information is needed to develop accurate thermodynamic models for arsenic scavenging by magnetite, similar to those for arsenic sorption on goethite.[28,29]

We recently reported spectroscopic evidence for a tridentate As(III) inner-sphere complex (^3C As(III)-surface complex) on {111} surfaces of nanoparticulate magnetite that formed in coprecipitation experiments.[13] This new surface complex explains EXAFS spectroscopic results on As(III) speciation after bioreduction of As-doped ferrihydrite into magnetite,[20] and it has also been reported for maghemite in ref 27 .

In the present study, we investigated the nature of sorbed As(III) species on nanoparticulate magnetite as a function of surface coverage, using extended X-ray absorption fine structure (EXAFS) spectroscopy. Two nanoparticulate magnetite samples—one with an average diameter of 11 nm that was prepared abiotically and one with an average diameter of 34 nm that was prepared via a biotic synthesis pathway—were compared to evaluate the role of particle size and As(III) surface coverage on surface reactivity with respect to arsenic. Special care was taken to preserve anoxic conditions during the sorption experiments and

EXAFS data collection in order to preserve the oxidation state of both As and Fe on the magnetite surface. We found that As(III) is adsorbed as dominantly inner-sphere, tridentate complexes on the {111} surface at surface coverages of < 2 $\mu mol/m^2$, whereas an As(III)-rich amorphous surface precipitate forms at higher As(III) surface coverages.

Materials and Experiment

Magnetite Samples. The biogenic magnetite sample, referred to as "Mt-bio", was prepared via the reduction of lepidocrocite (γ-FeOOH) by the ATCC 8071 strain of the dissimilatory Fe-respiring bacterium *Shewanella putrefaciens* at 303 K and an initial pH of 7.6 in the presence of sodium methanoate ($NaHCO_2$) as the electron donor. Anthraquinone 2,6-disulfonate (AQDS), an electron shuttle, was added to enhance bacterial reduction of the ferric oxyhydroxide.[17,18] The solid phase was harvested by centrifugation ($10000g$, 10 min), washed twice in O_2-free Milli-Q water, and vacuum-dried for 48 h. Previous studies using Mössbauer spectroscopy[17] and X-ray magnetic circular dichroism[18] indicated that the biogenic magnetite sample consists of close-to-stoichiometric magnetite with hyperfine parameters close to those of natural magnetites[30,31] and with a slight excess of octahedral Fe^{2+} at the particle surface as detected by electron yields.[18]

The abiotic magnetite sample, referred to as "Mt-cp", was prepared by aqueous coprecipitation of Fe^{2+} and Fe^{3+} ions in a Jacomex glovebox under N_2 atmosphere (< 50 ppm of O_2), following the procedure reported in ref 13. Iron chloride solutions (1 M) were prepared at 293 K by dissolving hydrated Fe(II) or Fe(III) chloride powders (> 99.9% purity level) in O_2-free water, previously obtained from Milli-Q water purged with N_2 (Alphagaz 1, Air Liquide) at 353 K. NaOH solution (1 N) was prepared similarly from NaOH pellets. After 5 mL of the 1 M $FeCl_2 \cdot 4H_2O$ solution was mixed with 10 mL of 1 M $FeCl_3 \cdot 6H_2O$ solution in a glass serum bottle, the pH was adjusted to 7.2 by adding appropriate quantities of the 1 N NaOH solution. This near-neutral pH value was chosen to be consistent with the pH of our sorption experiments and with natural waters' pH range. The bottle was sealed with a butyl rubber stopper and was agitated for 24 h at 293 K. The suspension was then centrifuged, and the resulting black powder was dried under vacuum in the glovebox for later X-ray diffraction (XRD) analysis, high-resolution transmission electron microscopy (HRTEM), and N_2 BET analysis. The supernatant was filtered through a 0.22 μm membrane, acidified, and stored in the glovebox prior to further solution analysis.

HRTEM micrographs of the two magnetite samples indicate octahedral crystals with dominant {111} facets and average diameters of 31 $\pm$ 7 and 11 $\pm$ 5 nm for Mt-bio and Mt-cp, respectively (Figure 1a). Surface areas (34 $\pm$ 4 and 103 $\pm$ 3 m^2/g for Mt-bio and Mt-cp, respectively) derived from mean coherent domain (MCD) sizes (34 $\pm$ 1 and 11.3 $\pm$ 0.3 nm for Mt-bio and Mt-cp, respectively) determined by Rietveld refinement of XRD powder patterns were higher than surface areas determined by the N_2 BET method (28 $\pm$ 2 and 83 $\pm$ 2 m^2/g for Mt-bio and Mt-cp, respectively). As shown by HRTEM observations, this discrepancy in surface areas determined by the two approaches is likely related to aggregation of single crystals in the powder samples used for BET analyses, as was also observed for smaller (6 nm) maghemite particles.[27] Although our sorption experiments were conducted on sonicated suspensions of the magnetite powders, we used the BET surface areas to estimate surface coverages in order to be consistent with previous studies.[24-27]

Sorption Experiments. Sorption experiments were performed at an ionic strength of 0.1 N NaCl. Solutions of NaCl,

(16) Lovley, D. R.; Stolz, J. F.; Nord, G. L.; Phillips, E. J. P. *Nature* **1987**, *330*, 252–254.

(17) Ona-Nguema, G.; Abdelmoula, M.; Jorand, F.; Benali, O.; Géhin, A.; Block, J.-C.; Génin, J.-M. R. *Environ. Sci. Technol.* **2002**, *36*, 16–20.

(18) Carvallo, C.; Sainctavit, P.; Arrio, M.-A.; Menguy, N.; Wang, Y.; Ona-Nguema, G.; Brice-Profeta, S. *Am. Mineral.* **2008**, *93*, 880–885.

(19) Glasauer, S.; Weidler, P. G.; Langley, S.; Beveridge, T. J. *Geochim. Cosmochim. Acta* **2003**, *67*, 1277–1288.

(20) Coker, V. S.; Gault, A. G.; Pearce, C. I.; van der Laan, G.; Telling, N. D.; Charnock, J. M.; Polya, D. A.; Lloyd, J. R. *Environ. Sci. Technol.* **2006**, *40*, 7745–7750.

(21) Pedersen, H. D.; Postma, D.; Jakobsen, R. *Geochim. Cosmochim. Acta* **2006**, *70*, 4116–4129.

(22) Kocar, B., D.; Herbel, M. J.; Tufano, K. J.; Fendorf, S. *Environ. Sci. Technol.* **2006**, *40*, 6715–6721.

(23) Tufano, K. J.; Fendorf, S. *Environ. Sci. Technol.* **2008**, *42*, 4777–4783.

(24) Yavuz, C. T.; Mayo, J. T.; Yu, W. W.; Prakash, A.; Falkner, J. C.; Yean, S.; Cong, L.; Shipley, H. J.; Kan, A.; Tomson, M.; Natelson, D.; Colvin, V. L. *Science* **2006**, *314*, 964–967.

(25) Yean, S.; Cong, L.; Yavuz, C. T.; Mayo, J. T.; Yu, W. W.; Kan, A. T.; Colvin, V. L.; Tomson, M. B. *J. Mater. Res.* **2005**, *20*, 3255–3264.

(26) Mayo, J. T.; Yavuz, C.; Yean, S.; Cong, L.; Shipley, H.; Yu, W.; Falkner, J.; Kan, A.; Tomson, M.; Colvin, V. *Sci. Technol. Adv. Mater.* **2007**, *8*, 71–75.

(27) Auffan, M.; Rose, J.; Proux, O.; Borschneck, D.; Masion, A.; Chaurand, P.; Hazemann, J. L.; Chaneac, C.; Jolivet, J. P.; Wiesner, M. R.; Van Geen, A.; Bottero, J. Y. *Langmuir* **2008**, *24*, 3215–3222.

(28) Stachowicz, M.; Hiemstra, T.; van Riemsdijk, W. H. *J. Colloid Interface Sci.* **2006**, *302*, 62–75.

(29) Stachowicz, M.; Hiemstra, T.; van Riemsdijk, W. H. *J. Colloid Interface Sci.* **2008**, *320*, 400–414.

(30) Vandenberghe, R. E.; Barrero, C. A.; da Costa, G. M.; Van San, E.; De Grave, E. *Hyperfine Interact.* **2000**, *126*, 247–259.

(31) Vayssieres, L.; Chaneac, C.; Tronc, E.; Jolivet, J. P. *J. Colloid Interface Sci.* **1998**, *205*, 205–212.
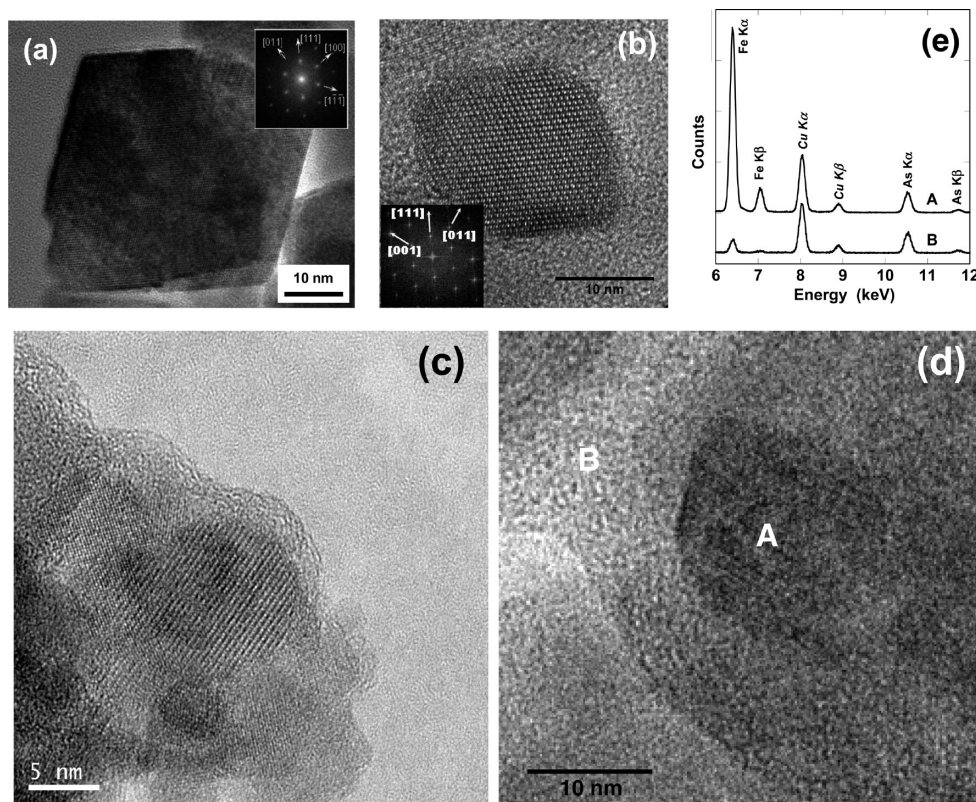
Figure 1. HRTEM images of selected magnetite samples: (a) an octahedral crystal of biogenic magnetite (Mt-bio) obtained upon anaerobic reduction of lepidocrocite by *Shewanella putrefaciens*, exhibiting well-developed {111} crystallographic faces; the corresponding electron diffraction pattern along the [011] zone axis is also displayed in the inset; (b) a cuboctahedral crystal of an Mt-cp magnetite sample with well developed {111} facets, obtained by coprecipitating Fe^{2+} and Fe^{3+} ions at neutral pH; the corresponding electron diffraction pattern along the [011] zone axis is displayed; (c) sample As(III)/Mt-cp 1.61 $\mu mol/m^2$ showing a thin amorphous coating (<3 nm) surrounding some magnetite particles; (d) sample As(III)/Mt-cp 10.1 $\mu mol/m^2$ showing a thick (up to 10 nm) amorphous coating surrounding magnetite particles; (e) EDXS analysis of selected points in image (d) ((A) a magnetite particle and (B) the arsenic-rich coating; the Cu signal arises from the carbon-coated copper grid used as the sample holder).

NaOH, and sodium arsenate or sodium arsenite were prepared in O_2-free water obtained from Milli-Q water purged with N_2 (Alphagaz 1, Air Liquide) at 353 K. Adsorption experiments were carried out in a N_2 atmosphere in a Jacomex glovebox. Suspensions of the magnetite particles were prepared by the addition of 0.5 g of magnetite in 38 mL of NaCl solution for all samples, except for two Mt-cp samples for which 0.37 g of magnetite was added (Table 1). An arsenite stock solution containing 66.8 mM As(III) was prepared by dissolving 0.868 g of $NaAsO_2$ (Sigma) or 2.084 g in 100 mL of O_2-free water. Various volumes of the arsenite stock solution were added to magnetite suspensions to obtain initial As concentrations reported in Table 1, which are below arsenolite (As_2O_3) solubility at pH 7, 178 mM.[32] For all samples, the pH was adjusted to 7.2 ± 0.3 with appropriate volumes of 1 N NaOH or 0.12 M HCl (Table 1) after arsenic addition. Finally, an appropriate volume of NaCl solution was added to obtain a final volume of 40 mL. The flasks were incubated for 24 h in darkness at 293 K and agitated at 200 rpm. After 24 h of incubation, the final pH of the suspensions, measured with a glass combination pH electrode, was 7.4 ± 0.5 for all experiments (Table 1). Solids were harvested by centrifugation (10000*g*, 15 min) and vacuum-dried for 6 days under vacuum for EXAFS analysis. To determine final surface coverage after 24 h of reaction time, the supernatants were filtered through a 0.22 μm membrane and acidified with HNO_3 in the glovebox to avoid precipitation of iron oxides that would result in a decrease in concentration of iron and arsenic in the solution. Fe concentrations were determined by inductively coupled plasma-atomic

emission spectroscopy (ICP−AES) performed on a Jobin-Yvon JY 238 Ultrace spectrometer, and As concentrations were determined by graphite furnace atomic absorption spectrometry (GFAAS) on a Unicam 989 QZ spectrometer. The detection limits were 0.018 μM and 0.03 μM for Fe and As, respectively. Final coverage values reported in Table 1 are used to refer to the samples thereafter.

EXAFS Data Collection and Analysis. EXAFS data were recorded on vacuum-dried samples in fluorescence detection mode at the As−K edge (11869 eV) using a Si(220) double-crystal monochromator on beamline 11-2 at the Stanford Synchrotron Radiation Lightsource (SSRL). Data were collected using a 30-element Ge array detector, and elastic scattering and Fe fluorescence were minimized using a 3 or 6 $\triangle \mu$ Ge filter. For Mt-cp sorption samples at As(III) surface coverages of ≤3.9 $\mu mol/m^2$, the energy resolution was ≈1.0 eV, with a beam height of 2 mm. For all Mt-bio sorption samples and for Mt-cp samples at As(III) surface coverages of ≥4.9 $\mu mol/m^2$, the energy resolution was ≈0.4−0.5 eV with a beam height of 250 μm, which was achieved using a vertical focusing mirror. The beam width was limited to 500 μm using vertical slits. Energy was calibrated using a double-transmission setup in which the As K-edge spectrum of the samples and that of a scorodite ($FeAsO_4 \cdot 2H_2O$) reference sample were simultaneously recorded. The absorption maximum of the As(V)-edge was chosen at 11875.0 eV. To preserve anoxic conditions, the samples were transferred from the glovebox to a liquid N_2 bath and then to a modified Oxford liquid He cryostat, where they were placed in a He atmosphere. Photo-oxidation of As(III) under the X-ray beam was limited by recording all data at 10−15 K using the Oxford cryostat and by automatically moving

(32) Neuberger, C. S.; Helz, G. R. *Appl. Geochem.* **2005**, *20*, 1218–1225.

Table 1. Sorption Data for the Samples Studied[a]

	pH$_{final}$	[As]$_{added}$ (μM)	Mt$_{added}$ (g)	[As]$_{final}$ (μM)	[As]$_{adsorbed}$ (μM)	final coverage[b] (μmol m^{-2})	[Fe]$_{final}$ (μM)
Mt-bio As(III) 4.8 μmol/m^2	7.6	1670	0.5	na[c]	na	na	na
Mt-bio As(III) 1.9 μmol/m^2	7.6	500	0.37	0.15 (5)	499.85 (5)	1.9 (2)	28.9 (2)
Mt-bio As(III) 0.19 μmol/m^2	7.5	50	0.37	< 0.03	50.00 (5)	0.19 (2)	24.1 (2)
Mt-cp As(III) 10.1 μmol/m^2	6.9	20541	0.5	10053 (1)	10488 (1)	10.1 (2)	4.4 (1)
Mt-cp As(III) 8.2 μmol/m^2	7.4	10354	0.5	1813 (1)	8541 (10)	8.2 (2)	1.1 (1)
Mt-cp As(III) 4.9 μmol/m^2	7.4	5130	0.5	52 (1)	5078 (1)	4.9 (1)	6.6 (1)
Mt-cp As(III) 3.8 μmol/m^2	7.4	4000	0.5	14.9 (1)	3985.1 (1)	3.8 (1)	na
Mt-cp As(III) 1.61 μmol/m^2	7.2	1670	0.5	1.13 (5)	1668.87 (5)	1.61 (4)	96.4 (5)
Mt-cp As(III) 0.16 μmol/m^2	7.5	167	0.5	< 0.03	167.00 (3)	0.16 (1)	47.5 (3)
Mt-cp[d]	7.4	0	0.5	0	0	0	22.0 (2)

[a] Experiments were conducted under anoxic conditions in a total volume of 40 mL at an ionic strength of 0.1 N NaCl. BET surface areas of the Mt-bio and Mt-cp samples are 28 ± 2 and 83 ± 2 m^2 g^{-1}, respectively. MCD particle sizes determined from Rietveld refinement of XRD powder patterns are 34 ± 3 and 11.3 ± 0.3 nm. Standard deviations for the dissolved arsenic concentrations measured by GF-AAS are represented by the numbers in parentheses and refer to the last decimal place. [b] Final coverage determined from dissolved arsenic concentration in the supernatant after 24 h reaction. [c] na, not analyzed. [d] Blank experiment without arsenic.

the sample 1 mm between each EXAFS scan.[13,14,33,34] Between two and eight EXAFS scans were accumulated for each sample to obtain an adequate signal-to-noise ratio at $k_{max} = 14$ Å^{-1}. The EXAFS spectrum collected with the same setup on sample As-(III)/Mt-cp 1.6 μmol/m^2 was reported in an earlier publication.[13]

EXAFS spectra were extracted from the raw fluorescence data using the XAFS program.[35] Radial distribution functions (RDF) were obtained by Fourier transforming the $k^3\chi(k)$ EXAFS functions using a Kaiser−Bessel window within the 2.7−14 Å^{-1} k range, with a Bessel weight of 2.5. Least-squares fitting of the unfiltered $k^3\chi(k)$ functions was performed with the plane-wave formalism, using a Levenberg−Marquard minimization algorithm. Theoretical phase-shift and amplitude functions employed in this fitting procedure were calculated with the curved-wave formalism using the ab initio FEFF 8 code.[36] As−O and As−Fe phase-shift and amplitude functions were extracted from the tooeleite crystal structure.[37] The fit quality was estimated using a reduced χ^2 of the form

$$\chi^2_{FT} = \frac{N_{ind}}{(N_{ind} - p)n} \sum_{i=1}^{n} (\|FT\|_{exptl_i} - \|FT\|_{calcd_i})^2$$

with $N_{ind} = (2\Delta k \Delta R)/\pi) =$ the number of independent parameters, p the number of free fit parameters, n the number of data points fitted, and $\|FT\|_{exptl}$ and $\|FT\|_{calcd}$ the experimental and theoretical Fourier transform magnitudes within the 0−8 Å R range of the k^3-weighted EXAFS. The number of allowable independent parameters is 57 ($\Delta k = 11.3$ and $\Delta R = 8$), and our fits included 17 variable parameters at most.

Results

Sorption Results. The quantities of adsorbed arsenite determined from supernatant analyses are reported in Table 1. Corresponding arsenite sorption isotherms (Figure 2a) are within an order of magnitude of results from previous studies,[24,27] but show lower sorption efficiency than on dispersed nanomagnetite at high As(III) surface coverages[24] and higher sorption efficiency than on nanomaghemite at low surface coverages.[27] More than 98% arsenic sorption was achieved for surface coverages of up to 3.8 μmol/m^2 on both Mt-cp and Mt-bio substrates. For the higher coverages investigated on the Mt-cp substrate, the percentage of adsorbed

As(III) decreased dramatically to 82% at 8.2 μmol/m^2 and to 51% at 10.1 μmol/m^2. Such a drop in sorption efficiency at high coverage has also been observed in previous studies,[24,27] although with a lower slope in the case of dispersed nanomagnetite[24] (Figure 2a). In the present experiments on magnetite, this drop in sorption efficiency is explained by surface precipitation of As(III), as discussed below. The equilibrium concentration of dissolved As-(III) in our experiments was below the MCL recommended by the WHO (10 μg/L) only for our lowest coverage samples (i.e., 0.16 and 0.19 μmol/m^2 for the Mt-cp and Mt-bio substrates, respectively).

The concentration of dissolved iron (Table 1) at the end of the 24 h sorption experiments varied as a function of As(III) coverage and as a function of the substrate (Table 1), the strongest variations being observed for the Mt-cp substrate. For this substrate, the concentration of dissolved iron increased from 22 μM in the As-free experiment to 98 μM in the 1.61 μmol/m^2 experiment (1669 μM adsorbed As(III)) and decreased significantly with increasing As(III) surface coverage, down to 4 μM in the 10.1 μmol/m^2 experiment (10488 μM adsorbed As(III)). This range of dissolved iron concentration values is in reasonable agreement with expected magnetite solubility at room temperature at pH 7, as extrapolated from available high-temperature data.[38] Because these variations in dissolved Fe concentration were always > 20 times smaller than the quantity of adsorbed arsenic, such a low concentration of dissolved iron in our experiments is not expected to have influenced significantly As(III) sorption.

HRTEM Observations and EDXS Analyses. To better understand the drop in sorption efficiency at high As(III) surface coverages observed for the Mt-cp substrate, the intermediate and highest surface coverage samples (1.61 and 10.1 μmol/m^2, respectively) were characterized using HRTEM. Figure 1c displays a typical micrograph of sample As(III)/Mt-cp 1.61 μmol/m^2 and shows that magnetite nanocrystals are locally coated by a thin amorphous phase of 1−3 nm thickness. In the highest surface coverage sample studied, As(III)/Mt-cp 10.1 μmol/m^2, this coating is thicker (< 10 nm; Figure 1d) than in the As(III)/Mt-cp 1.61 μmol/m^2 sample (< 5 nm). This surface precipitate was absent in the As-free starting materials and has a ~15-times higher As/Fe ratio compared to the magnetite nanoparticles in the As(III)/Mt-cp 10.1 μmol/m^2 sample, as determined by EDXS analyses performed at the nanometer scale (Figure 1e). Moreover, the apparent As/Fe ratio in the surface precipitate might be underestimated by the EDXS analysis because of the difficulty of

(33) Ona-Nguema, G.; Morin, G.; Juillot, F.; Calas, G.; Brown, G. E., Jr. *Environ. Sci. Technol.* **2005**, *39*, 9147–9155.
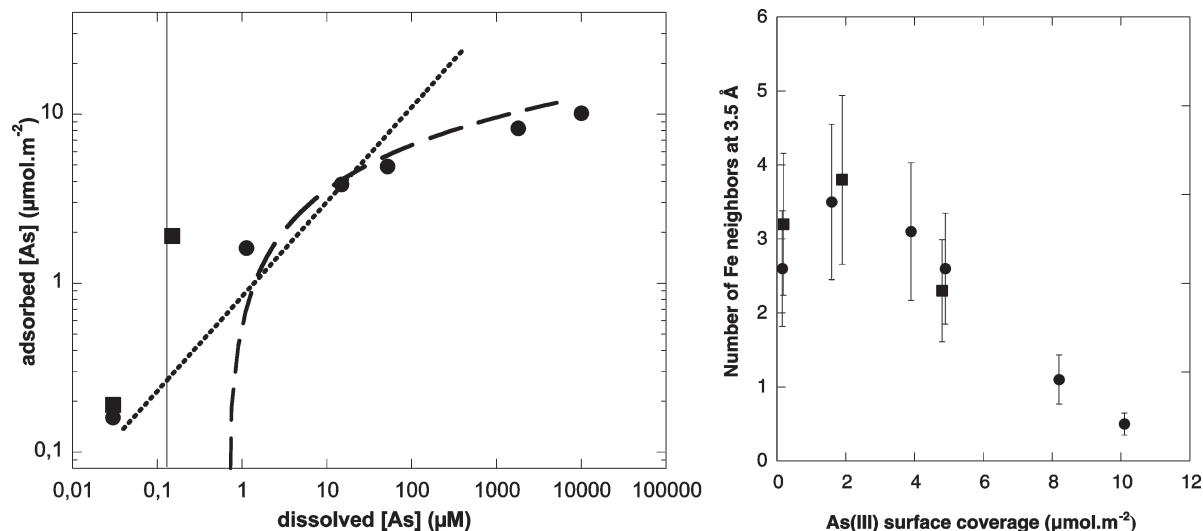
(34) Morin, G.; Ona-Nguema, G.; Wang, Y.; Menguy, N.; Juillot, F.; Proux, O.; Guyot, F.; Calas, G.; Brown, G. E., Jr. *Environ. Sci. Technol.* **2008**, *42*, 2361–2366.

(35) Winterer, M. *J. Phys. IV* **1997**, *7*, 243–244.

(36) Ankudinov, A. L.; Ravel, B.; Rehr, J. J.; Conradson, S. D. *Phys. Rev. B* **1998**, *58*, 7565–7576.

(37) Morin, G.; Rousse, G.; Elkaim, E. *Am. Mineral.* **2007**, *92*, 193–197.

(38) Beverskog, B.; Puigdomenech, I. *Corros. Sci.* **1996**, *38*, 2121–2135.

Figure 2. (a, left) Arsenic sorption isotherms at pH 7 ± 0.5 for the As(III)/Mt-Cp series (solid circles) and As(III)/Mt-bio (solid squares) compared with the regression curves reported in ref 24 for As(III) sorption onto 12 nm magnetite dispersed using a surfactant and in ref 27 for As(III) sorption on 6 nm maghemite. The MCL recommended by WHO for arsenic, that is, $10\,\mu g/L$, is indicated by a vertical line. (b, right) Variation in the number of Fe second neighbors at a distance of 3.5 Å determined by As K-EXAFS fitting as a function of As(III) surface coverage for the As(III)/Mt-cp samples (solid circles) and the As(III)/Mt-bio samples (solid squares).

analyzing such a thin coating without integrating the X-ray emission signal from the neighboring magnetite particle. However, the presence of a small amount of iron in the precipitate is consistent with the decrease of the dissolved iron concentration down to $4\,\mu M$ in this high As(III)-coverage sample. Because dissolved iron is expected to be mostly divalent at pH 7, these observations suggest that the surface precipitate mainly consists of an amorphous arsenite (hydr)oxide, which may have incorporated or sorbed a small amount of Fe(II). The oxidation state of iron in the precipitate could not be directly determined by electron energy loss spectroscopy because the thickness of the precipitate in the investigated samples was too small.

Arsenic Oxidation State. Arsenic K-edge X-ray absorption near-edge structure (XANES) spectra exhibit an absorption maximum at 11871.3 for As(III)-sorbed samples (Figures 3a and 4a). The As(V) content was below the detection limit of the XANES method ($\approx 5\%$).[39]

EXAFS Analysis. Arsenic K-edge EXAFS data for As(III) sorbed on Mt-bio and on Mt-cp are displayed in Figures 3b,c and 4b,c, respectively. Tables 2 and 3 list the fit results for the unfiltered, k^3-weighted EXAFS functions for As(III)/Mt-bio and As(III)/Mt-cp, respectively. For all samples, the first-neighbor contribution to the EXAFS was fit with $(2.6-3.4) \pm 0.5$ oxygen atoms at 1.78 ± 0.02 Å (Table 2). These coordination numbers and distances are consistent with a regular AsO_3 pyramid.[37] For all samples, second-neighbor contributions to the EXAFS were fit using As—Fe pairs at various distances and a multiple-scattering (MS) contribution corresponding to the six As—O—O—As paths within the AsO_3 pyramid (Tables 2 and 3). The numbers of neighbors associated with these MS contributions were fixed at the expected value of 6. The distances fit for this MS contribution range from 3.12 to 3.20 Å for As(III)/Mt sorption samples and thus agree with the corresponding As—O—O—As distances in the crystal structure of tooeleite (3.14 Å).[37]

Second-neighbor contributions are sharp in the As(III)/Mt sorption samples (Figures 2, 3, and 4) up to surface coverages of

about $4\,\mu mol/m^2$ and significantly decrease above this value. Indeed, as illustrated by the FT of the unfiltered, k^3-weighted EXAFS spectra (Figures 3c and 4c), the second-neighbor contributions ($R + \Delta R = 2.5-4.0$ Å) exhibit a similar shape for all As(III)/Mt sorption samples, with decreasing amplitude above 1.9 and $1.61\,\mu mol/m^2$ for Mt-bio and Mt-cp samples, respectively, and a dramatic drop in the number of second-neighbor Fe atoms above $3.8\,\mu mol/m^2$ for the Mt-cp samples. For all samples, this second-neighbor contribution to the EXAFS was fit by $0.5-3.8$ As—Fe pairs at a distance of 3.5 ± 0.04 Å and by $1.1-1.9$ As—Fe pairs at a distance of 3.7 ± 0.04 Å. The presence of the latter As—Fe contribution is related to the shoulder on the high-distance side of the FT peak centered at $R + \Delta R = 3.1$ Å. These distances are fully consistent with the ^3C hexanuclear, tridentate, corner-sharing surface complex identified recently,[13] where AsO_3 pyramids occupy vacant FeO_4 tetrahedral sites on the {111} surface of magnetite particles (Figure 5). Feff8 analysis of such clusters[13] indicates that As—Fe pairs at a distance of 3.5 ± 0.04 Å are related to the closest pyramid-octahedron distance (Figure 5a) and that As—Fe pairs at a distance of 3.7 ± 0.04 Å are related to the closest pyramid-tetrahedron distances (Figure 5b). Additional contributions at longer distances observed for all samples, except the two highest coverage Mt-cp samples, are also consistent with this cluster geometry and can be modeled by three dominant single and multiple scattering paths[13] (Tables 2 and 3). Best fits (Figures 3 and 4) were thus obtained using $0.6-1.7$ As—O—Fe paths at a distance of 5.5 ± 0.05 Å (Figure 5a,b), $0.6-1.8$ As—Fe pairs at a distance of 6.0 ± 0.05 Å (Figure 5b), and $0.0-1.1$ As—Fe pairs at a distance of 6.95 ± 0.07 Å (Figure 5a,b). The number of neighbors for these three paths is far below those expected for the ^3C surface complex (i.e., 10, 3, and 9, respectively[13]) likely because of destructive interference with other multiple scattering paths involving oxygen atoms. Consequently, the observed number of neighbors at such long distances is not reliable.

In contrast, the maximum number of second neighbors observed at 3.5 ± 0.04 Å ($N = 3.8 \pm 1.3$) and 3.7 ± 0.04 Å ($N = 1.6 \pm 0.5$) in the samples studied is closer to the theoretical values expected for the ^3C complex ($N = 6$ and 1, respectively, Figure 5a), but remains significantly lower than these theoretical values. For some samples, the observed ratio of the number of As—Fe pairs at

(39) Morin, G.; Juillot, F.; Casiot, C.; Bruneel, O.; Personne, J. C.; Elbaz-Poulichet, F.; Leblanc, M.; Ildefonse, P.; Calas, G. *Environ. Sci. Technol.* **2003**, *37*, 1705–1712.
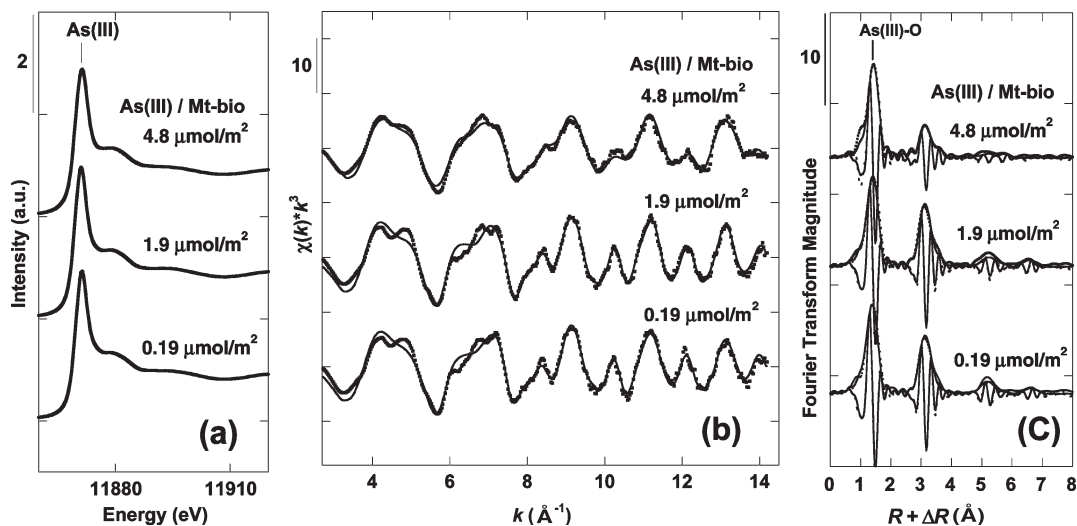
Figure 3. Arsenic K-edge data recorded at 10 K for As(III) sorbed onto Mt-bio as a function of As(III) surface coverage: (a) XANES data; (b) unfiltered k^3-weighted EXAFS data; (c) magnitude and imaginary part of the Fourier transform (FT). Note the decrease of the second-neighbor contribution to the EXAFS with increasing surface coverage (see text). Experimental and calculated k^3-weighted EXAFS curves (Table 3) as well as corresponding FT curves are displayed as dashed and solid lines, respectively.
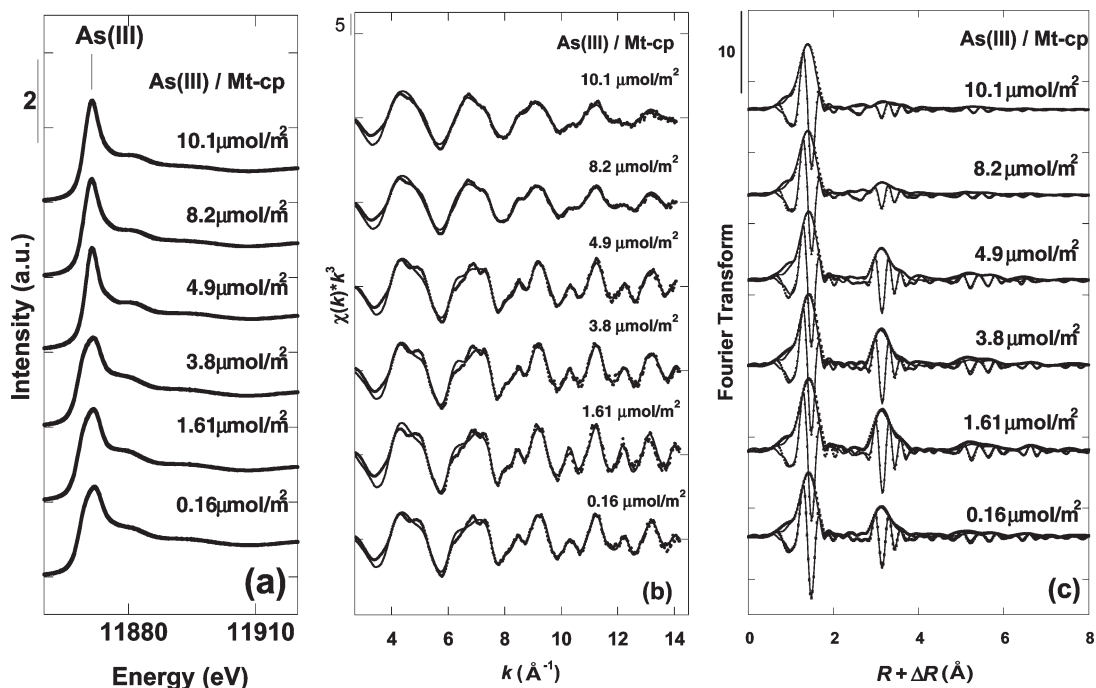
Figure 4. Arsenic K-edge data recorded at 10 K for As(III)-sorbed onto Mt-cp as a function of As(III) surface coverage: (a) XANES data (broadening of the XANES spectra for the three lowest surface coverage samples is caused by lower spectral resolution due to the use of an unfocused beam (see Methods and Experiment)); (b) unfiltered k^3-weighted EXAFS data; (c) magnitude and imaginary part of the Fourier transform (FT). Note the decrease of the second-neighbor contribution to the EXAFS with increasing surface coverage (see text). Experimental and calculated k^3-weighted EXAFS curves (Table 3) as well as corresponding FT curves are displayed as dashed and solid lines, respectively.

3.7 ± 0.04 Å relative to the ones at 3.5 ± 0.04 Å (Tables 2 and 3) is slightly greater than the ideal ratio of 1/6 expected for octahedral termination of the surface (Figure 5b). These differences are interpreted as being due to the formation of additional ^3C complexes at defective surface sites of the magnetite {111} surface, as discussed in the following section. Eventually, the number of second neighbors at the characteristic distance of the ^3C complexes (3.5 ± 0.04 Å) follows the same variation as a function of As(III)-coverage for both Mt-cp and Mt-bio substrates (Figure 2b), with a maximum around 2 μmol/m^2 and a dramatic decrease with increasing surface coverage. This similar behavior is

interpreted as a change in sorption processes as a function of surface coverage, as discussed in the following section.

Discussion

Arsenic Oxidation State. Although thermodynamic data predict that the reduction of Fe(III) to Fe(II) can be coupled with the oxidation of As(III) to As(V),[40] our XANES results indicate no measurable change in arsenic oxidation state (< 5%

(40) Vanysek, P. In *Handbook of Chemistry and Physics*, 76th ed.; Lide, D. R., Ed.; CRC Press: Boca Raton, FL, 1995.

Table 2. Results of Shell-by-Shell Fitting of Unfiltered EXAFS Data for the Samples of As(III) Sorbed on Mt-bio Magnetite Samples[a]

sample	R (Å)	N	σ (Å)	$\triangle E_0$ (eV)	χ^2_{FT}
Mt-bio As(III) 4.8 μmol m^{-2}	1.79	2.6 As−O	0.04	14	0.13
	3.20	6.0(f) As−O−O	−	−	
	3.52	2.3 As−Fe	0.06	−	
	3.72	1.3 As−Fe	−	−	
	5.50	0.6 As−O−Fe	−	−	
	6.03	1.0 As−Fe	−	−	
Mt-bio As(III) 1.9 μmol.m^{-2}	1.78	3.1 As−O	0.06	12	0.14
	3.17	6.0(f) As−O−O	−	−	
	3.51	3.8 As−Fe	0.06	-	
	3.71	1.6 As−Fe	−	−	
	5.53	1.3 As−O−Fe	−	−	
	5.94	0.8 As−Fe	−	−	
	6.94	0.9 As−Fe	−	−	
Mt-bio As(III) 0.19 μmol m^{-2}	1.77	3.2 As−O	0.06	11	0.14
	3.13	6.0(f) As−O−O	−	−	
	3.50	3.2 As−Fe	0.06	−	
	3.72	1.0 As−Fe	−	−	
	5.53	1.7 As−O−Fe	−	−	
	5.94	0.6 As−Fe	−	−	
	6.94	0.7 As−Fe	−	−	

[a] All distances can be assigned to a single dominant ^3C tridentate complex on the {111} surfaces of magnetite nanoparticles. R (Å), interatomic distance; N, number of neighbors; σ (Å), Debye−Waller factor, $\triangle E_0$ (eV) = difference between the user-defined threshold energy and the experimentally determined threshold energy, in electron volts; χ^2_{FT}, goodness of fit (see text). During the fitting procedure, all parameter values indicated by (−) were linked to the parameter value placed above in the table and those followed by (f) were fixed. Errors in R and N values, estimated from the fit of the tooeleite As K-edge EXAFS data (not shown), are ±10 and ±30%, respectively. Errors in σ and $\triangle E_0$ values are ±0.01 and ±3, respectively.

As(V)) in any of the sorption samples within 24 h following sorption on magnetite. This result is consistent with the absence of As(III) oxidation upon sorption onto Fe(II,III) (hydr)oxides under anoxic conditions[13,14] that prevent Fenton oxidation reactions.[41]

Evidence for a ^3C Arsenite Complexes on the {111} Magnetite Surface. The characteristic As−Fe distances of the tridentate, hexanuclear, corner-sharing ^3C surface complex (3.5 ± 0.04 and 3.7 ± 0.04 Å) on the magnetite {111} surface, accompanied by As−Fe MS contributions at long distances,[13] differ significantly from those of bidentate binuclear corner-sharing (^2C) surface complexes (3.38 ± 0.03 Å) and of bidentate, mononuclear, edge-sharing surface complexes (^2E) (2.95 ± 0.03 Å) observed for As(III) adsorption on hematite and ferrihydrite.[33] Arsenite also adsorbs in different modes on goethite and lepidocrocite (^2C and monodentate mononuclear ^1V complexes).[33,42] The present study demonstrates the formation of ^3C surface complexes upon sorption of arsenite at the surface of magnetite and suggests that the surface structure of magnetite nanoparticles provides specific adsorption sites for arsenite. Indeed, this ^3C As(III) surface complex was recently reported for As(III) coprecipitation with magnetite[13] and for As(III) sorption on maghemite at low surface coverages (~0.7 μmol/m^2)[27] with a slightly shorter As−Fe distance (3.41 ± 0.02 Å) than in the present study (3.50 ± 0.04 Å). We show here that the ^3C complex is important over a wide range of surface coverages (0.16−4.9 μmol/m^2)

(41) Hug, S. J.; Leupin, O. *Environ. Sci. Technol.* **2003**, *37*, 2734−2742.
(42) Manning, B. A.; Hunt, M. L.; Amrhein, C.; Yarmoff, J. A. *Environ. Sci. Technol.* **2002**, *36*, 5455−5461.

Table 3. Results of Shell-by-Shell Fitting of Unfiltered EXAFS Data for the Adsorption of As(III) Mt-cp Magnetite Samples[a]

sample	R (Å)	N	σ (Å)	$\triangle E_0$ (eV)	χ^2_{FT}
Mt-cp As(III) 10.1 μmol m^{-2}	1.78	3.1 As−O	0.07	13	0.07
	3.16	6.0(f) As−O−O	−	−	
	3.47	0.5 As−Fe	−	−	
	3.77	0.5 As−Fe	−	−	
	5.55	0.6 As−O−Fe	−	−	
	5.98	0.4 As−Fe	−	−	
	7.00	0.3 As−Fe−Fe	−	−	
Mt-cp As(III) 8.2 μmol m^{-2}	1.78	3.0 As−O	0.07	13	0.07
	3.17	6.0(f) As−O−O	−	−	
	3.48	1.1 As−Fe	−	−	
	3.72	0.4 As−Fe	−	−	
	5.52	0.5 As−O−Fe	−	−	
	5.99	0.8 As−Fe	−	−	
	7.05	0.4 As−Fe−Fe	−	−	
Mt-cp As(III) 4.9 μmol m^{-2}	1.78	3.1 As−O	0.06	16	0.11
	3.13	6.0(f) As−O−O	−	−	
	3.50	2.6 As−Fe	−	−	
	3.72	1.2 As−Fe	−	−	
	5.50	1.1 As−O−Fe	−	−	
	6.00	1.8 As−Fe	−	−	
	6.98	0.7 As−Fe−Fe	−	−	
Mt-cp As(III) 3.8 μmol m^{-2}	1.77	3.2 As−O	0.06	16	0.12
	3.13	6.0(f) As−O−O	−	−	
	3.50	3.1 As−Fe	0.06	−	
	3.70	1.3 As−Fe	−	−	
	5.49	1.0 As−O−Fe	−	−	
	5.99	1.8 As−Fe	−	−	
	6.95	0.5 As−Fe−Fe	−	−	
Mt-cp As(III) 1.61 μmol m^{-2}	1.79	3.4 As−O	0.07	17	0.13
	3.12	6.0(f) As−O−O	−	−	
	3.51	3.5 As−Fe	0.06	−	
	3.73	1.9 As−Fe	−	−	
	5.53	1.2 As−O−Fe	−	−	
	6.01	1.5 As−Fe	−	−	
	6.97	1.1 As−Fe−Fe	−	−	
Mt-cp As(III) 0.16 μmol m^{-2}	1.77	2.9 As−O	0.06	16	0.11
	3.16	6.0(f) As−O−O	−	−	
	3.50	2.6 As−Fe	0.06	−	
	3.72	1.1 As−Fe	−	−	
	5.50	0.7 As−O−Fe	−	−	
	6.03	1.2 As−Fe	−	−	
	6.94	0.7 As−Fe−Fe	−	−	

[a] All distances can be assigned to a ^3C tridentate complex on the Mt {111} surface of the magnetite particles. The decrease of the number of Fe neighbors at 3.5 Å in the highest surface coverage samples is related to the formation of an As-rich surface precipitate. R (Å), interatomic distances; N, number of neighbors; σ (Å), Debye−Waller factor, $\triangle E_0$ (eV) = difference between the user-defined threshold energy and the experimentally determined threshold energy, in electron volts; χ^2_{FT} = goodness of fit (see text). During the fitting procedure, all parameter values indicated by (−) were linked to the parameter value placed above in the table and those followed by (f) were fixed. Errors in R and N values, estimated from the fit of the tooeleite As K-edge EXAFS data (not shown), are ±10 and ±30%, respectively. Errors in σ and $\triangle E_0$ values are ±0.01 and ±3, respectively.

for As(III) sorption on nanomagnetite synthesized via both biotic and abiotic pathways (Figure 2b). In addition, observation of this ^3C As(III) surface complex strongly suggests that the octahedral termination dominates the {111} faces of our magnetite nanoparticles in water, which is consistent with the most recent

(a)

(b)
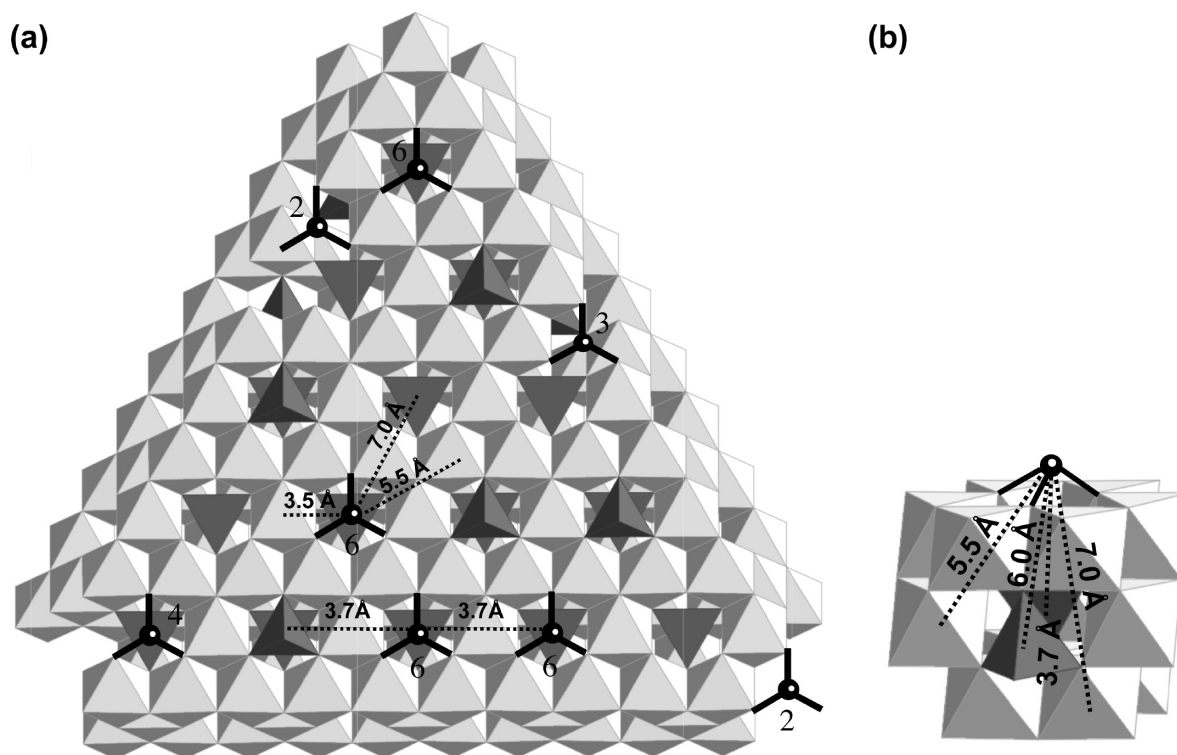
Figure 5. Proposed structural model for the As(III) tridentate, hexanuclear, corner-sharing complexes (^3C) on the {111} surface of magnetite. In these complexes, the As(III)O$_3$ pyramids (black) occupy vacant FeO$_4$ tetrahedral sites (dark gray) on the octahedrally terminated {111} surface of the magnetite particles: (a) top view; (b) side view. All As–Fe distances expected for this complex are consistent with EXAFS data (Tables 2 and 3). The number of Fe neighbors around arsenite at ~3.5 Å are reported for each sorbed arsenite molecule and can vary from 6 for the ideal ^3C complex on the octahedrally terminated surface to 2 on defect sites. Such sites can occur, for instance, on the edges, steps, and corners of the {111} surface. This decrease in the number of Fe neighbors around arsenic at defect sites can explain the lower number of As–Fe pair correlations observed by EXAFS for the lowest surface coverage samples (Figure 2b). The excess of As–Me pairs observed by EXAFS at a distance of 3.7 Å could be due to the presence of adjacent ^3C complexes and of additional surface FeO$_4$ tetrahedra.

structural study of the hydrated magnetite {111} surface.[43] More precisely, the proposed hydrated magnetite (111) surface structure derived from crystal truncation rod diffraction data by Petitto et al.[43] consists of 75% octahedral domains and 25% mixed tetrahedral–octahedral domains. Accordingly, the presence of some Fe(III)O$_4$ tetrahedra in their normal crystallographic position on the magnetite {111} surface could explain the slight excess of As–Fe pairs at an EXAFS-derived distance of 3.7 ± 0.04 Å in our arsenite sorption samples (Figure 5b; Tables 2 and 3). In addition, the excess of second neighbors observed at this distance could also be partly due to As–As pair correlations, which are difficult to distinguish from As–Fe pair correlations because of similar backscattering from As and Fe atoms at this distance, especially when present in such low quantities (< 2 neighbors). A similar fit quality was obtained by including either As or Fe atoms at this distance (data not shown). Moreover, significant proportions of AsO$_3$ pyramids are expected to sorb to adjacent vacant tetrahedral sites on the {111} surface. Indeed, assuming all of these tetrahedral sites are initially vacant and considering a random distribution of As(III)-sorbed species over these sites (binomial law), the probabilities of finding at least one As(III) at an adjacent site around a sorbed As(III) surface complex are ~0.15 and ~0.3 for As(III) surface coverages of 0.16 and 1.61 μmol/m^2, respectively. The theoretical number of neighbors

at 3.7 Å would thus be ~1.15 and ~1.30, respectively, which is slightly lower than the observed values for the Mt-cp samples (N = 1.1 and 1.9; Table 3). Similar conclusions can be drawn for the Mt-bio samples (Table 2). Altogether, these results suggest that both Fe and As neighbors on the {111} magnetite surface contribute to the EXAFS-derived distance at 3.7 Å around adsorbed As(III) atoms.

The two lowest surface coverage samples investigated (0.16 and 0.19 μmol/m^2) showed a slight decrease in the number of As–Fe pair correlations at 3.5 Å (N = 2.6 ± 0.8 Fe and 3.2 ± 0.9 Fe) (Figure 2b; Table 3). Such a decrease could be interpreted as being due to destructive interferences with other type of surface complex with differing As–Fe distances. However, because we do not observe any As–Fe pair correlations other than those characteristic of the ^3C complex in these samples, we interpret this decrease in second-neighbor contributions at 3.5 Å as being due to the formation of surface complexes exhibiting the same dominant As–Fe distance at 3.5 Å as the ^3C complex, but at defective sites with fewer FeO$_6$ octahedra than the ideal ^3C complex. Such defective sites where arsenite may bond to only two, three, or four FeO$_6$ octahedra could occur, for instance, at the edges of {111} surfaces and/or close to octahedral iron vacancies (Figure 5a). In such defect sites, some OH groups are singly coordinated to iron and are thus expected to have higher affinity for arsenite than doubly coordinated OH groups of the ideal octahedral termination of the {111} surface. Such difference in affinity could explain the predominance of defect sites at the lowest surface coverages investigated (0.16 and 0.19 μmol/m^2), which

(43) Petitto, S. C.; Tanwar, K.; Ghose, S. K.; Eng, P.; Toney, M. F.; Trainor, T. P. *Abstracts of Papers*, 232nd ACS National Meeting, San Francisco, CA, Sept 10–14; American Chemical Society: Washington, DC, 2006.

represent only $\sim$3% of a theoretical AsO_3 monolayer on an octahedrally terminated surface {111}.

Evidence for As(III)-Fe-Containing Surface Precipitates and Their Influence on the Solubility of Sorbed Arsenite. Our As(III) sorption data on the Mt-cp substrate can be approximated by a Freundlich-type isotherm for surface coverage above 3.8 μmol/m^2 (Supporting Information Figure SI-4), which may be consistent with heterogeneous precipitation.[44,45] Moreover, several lines of evidence indicate the presence of an amorphous As(III)-Fe-containing precipitate in the As(III)/Mt sorption samples. The first is direct observation by HRTEM imaging of this amorphous phase as a coating on magnetite nanoparticles in samples Mt-cp 1.61 μmol/m^2 and 10.1 μmol/m^2 (Figure 1c,d). The As:Fe ratio of this precipitate is significantly higher than that of the magnetite nanoparticle as revealed by EDXS analysis (Figure 1e). The second line of evidence is less direct and comes from the observation that the number of second-neighbor iron atoms around As at an As–Fe distance of 3.5 $\pm$ 0.05 Å (characteristic of the ^3C complex) is lower than the theoretical value of 6 Fe second neighbors for all of the As(III)/Mt sorption samples examined. The low number of Fe second neighbors at 3.5 Å for the lowest surface coverage samples can be explained by the presence of arsenite surface complexes at defective sites, as discussed above. In contrast, the systematic decrease in the number of Fe second neighbors around As with increasing surface coverage above $\sim$2 μmol/m^2 observed for both Mt-cp and Mt-bio substrates (Figure 2b) is explained by the formation of the amorphous As(III)-Fe-containing precipitate observed by HRTEM (Figure 1c,d). Indeed, increasing amounts of this As(III)-rich amorphous phase are expected to result in a disordered second shell that is not easily detected or quantified by EXAFS spectroscopy. Moreover, the EXAFS signal from this precipitate could negatively interfere with the signal from the ^3C complex. Formation of the surface precipitate in our highest surface coverage samples (8.2 and 10.1 μmol/m^2) is likely related to the excess of As(III) with respect to the maximum site density (3.2 sites/nm^2 or 5.3 μmol/m^2) of vacant tetrahedral iron sites for the ideal octahedral termination of the (111) magnetite surface. However, the decrease in abundance of the ^3C complexes above $\sim$2 μmol/m^2 (Figure 2b) also suggests that formation of the surface precipitate begins before the As(III) coverage reaches this maximum site density. Such early formation of the surface precipitate might be explained by a limit on the number of vacant tetrahedral sites on the surface that can be occupied by Fe atoms, which is consistent with the surface structure proposed by Petitto et al.[43] Auffan et al.[27] also reported the presence of tetrahedral Fe atoms at the surface of maghemite and proposed that the occupancy of tetrahedral Fe sites decreases with increasing particle size. Our data do not confirm this result in the case of magnetite because the contributions of As(III) ^3C complexes are similar for the two particle sizes studied (Mt-bio, 34 nm, and Mt-cp, 11 nm) at similar As(III) surface coverages (Figure 2b).

Precipitation of an amorphous As(III)-Fe-containing solid at the surface of magnetite has a dramatic influence on the stability of sorbed As(III). Figure 2a shows that the dissolved arsenic concentration in equilibrium with Mt-cp increases to >10 μM (0.075 mg/L) for As(III) surface coverage values above 3.8 μmol/m^2, and it reaches 1.8 mM (135 mg/L) and 10 mM (750 mg/L) for surface coverage values of 8.2 and 10.1 μmol/m^2, respectively (Figure 2b). The apparent solubility of the observed As(III)-rich

surface precipitate, although lower than that of arsenolite (178 mM),[32] makes magnetite a less effective sorbent for As decontamination of natural waters when As(III) is present at surface coverages of >5 μmol/m^2. In contrast, our data show that As(III)-monomer ^3C surface complexes, which dominate at surface coverages of <2 μmol/m^2, are highly stable and result in a reduction of As(III) concentrations below the As MCL of 10 μg/L at surface coverages of <0.2 μmol/m^2 for both magnetite sorbents studied. This sorption efficiency at very low coverage is thought to be mostly related to the formation of arsenite surface complexes at highly reactive defect sites (Figure 5a).

Comparison with Arsenite Sorption on Maghemite. In the present study, the ^3C complex was the only one observed by EXAFS spectroscopy on magnetite (111) surfaces over a wide range of surface coverages (0.16–4.9 μmol/m^2). We attribute this consistency in surface complex type to a well-defined magnetite surface termination with one dominant type of adsorption site for As(III). In contrast, a variety of As(III) surface complexes (^2E, ^2C, and ^1V) were observed on maghemite (111) at As(III) coverages of 3–4 μmol/m^2,[34] whereas the ^3C complex was reported only at low coverage (0.7 μmol/m).[27] One possible explanation for this difference between magnetite and maghemite at intermediate As(III) surface coverages may involve differences in their hydrated surface structures. Indirect evidence of structural disorder on the maghemite (111) surface was indicated by weak As–Fe pair correlations consistent with a range of As–Fe distances (2.9–3.5 Å) at As(III) surface coverages of 3.0 and 4.2 μmol/m^2.[34] Such structural disorder could indeed lead to a variety of surface sites and thus to a variety of As(III) surface complexes on maghemite. In addition, evidence for the formation of an As(III)-surface precipitate on magnetite in our high-coverage sorption samples suggests that a similar process could occur at the maghemite surface. This hypothesis is supported by the similarity of the As(III)-sorption isotherms for magnetite and maghemite at high surface coverage values (see ref 27 and this study), as well as by the weak second-neighbor contribution observed by Auffan et al.[27] in their EXAFS analysis of a high coverage As(III)/maghemite sorption sample (13 μmol/m^2). Further HRTEM examination of such samples would help to detect the possible formation of such a surface precipitate at the maghemite surface upon arsenite sorption.

Conclusions

Detailed EXAFS analysis of sorbed As(III) species at the surface of nanomagnetite reveals that the high affinity of As(III) for the magnetite surface is related to the formation of highly stable ^3C As(III) complexes in which AsO_3 pyramids occupy vacant tetrahedral sites at the {111} surface of magnetite particles. These complexes, when they form at reactive defect sites for surface coverage values below 0.2 μmol/m^2, can maintain dissolved As concentration below the As MCL. In addition to these surface complexes, an amorphous As(III)-rich surface precipitate forms at high As(III) surface coverages. This surface precipitate begins to form at surface coverage of $\sim$2 μmol/m^2 and becomes the major As(III) species for surface coverage values of >4 μmol/m^2. The high solubility of this amorphous surface precipitate (10 mM H_3AsO_3 at pH 7), although 18 times lower than that of arsenolite (As_2O_3),[32] helps to explain the dramatic increase of dissolved As concentrations at high As(III) surface coverage. The formation of this surface precipitate also explains the exceptional sorption capacity of magnetite at As(III) coverages of >10 μmol/m^2, and it could also explain the hysteretic behavior of arsenite sorption–desorption on nanomagnetite reported in ref 26. These results

(44) Li, L.; Stanforth, R. *J. Colloid Interface Sci.* **2000**, *230*, 12–21.
(45) Sperlich, A.; Werner, A.; Genz, A.; Amy, G.; Worch, E.; Jekel, M. *Water Res.* **2005**, *39*, 1190–1198.

should be useful in developing models of As(III) surface complexation on magnetite and As transport, particularly in anoxic zones of soils and aquifers, as well as in putative water treatment processes.

Supporting Information Available: Figures SI-1 and SI-2 display additional HRTEM images for samples Mt-cp As(III) 1.61 μmol/m^2 and Mt-cp As(III) 10.1 μmol/m^2, respectively; Figure SI-3 displays XRD patterns of the Mt-bio and Mt-cp samples together with their Rietveld fit; and Figure SI-4 displays a log–log diagram of the sorption isotherm for the Mt-cp series. This material is available free of charge via the Internet at http://pubs.acs.org.